Integrated Modeling Structural Tools for the Giant Magellan Telescope Design Effort

David Schwartz
Giant Magellan Telescope
465 N. Halstead Street, Suite 250
Pasadena, CA 91107
310-968-0583
dschwartz@gmto.org

Kaylee Feigum
Accel Robotics
4250 Executive Square
kaylee@accelrobotics.com

Peter M. Thompson
Systems Technology, Inc.
13766 Hawthorne Blvd
Hawthorne, CA 90250
310-679-2281
pthompson@systemstech.com

Clark Briggs
ATA Engineering Inc.
13290 Evening Creek Dr S
San Diego, CA 92128
848-480-2042
clark.briggs@ata-e.com

Abstract— **The Giant Magellan Telescope (GMT) is an advanced Extremely Large Telescope and is being designed for broad wavelength coverage and maximum sensitivity in pursuit of several high priority cosmology science objectives. The GMT will use large primary mirror segments to provide well corrected wavefronts and a very fast optical system with a 20-arcminute diameter field of view. It will have a direct Gregorian optical prescription and deformable secondary mirrors to implement adaptive optics. The project timeline leads to initial commissioning with early instruments by 2023.**

The Systems Engineering group, along with the chief engineer, is developing and flowing down science and operational requirements and is the guardian of the performance budget. An integrated performance model of the telescope is being developed to support requirements derivation, performance assessment and trade studies that drive telescope architecture decisions. This model has four key elements; a structural plant model which exhibits the complex dynamics of the telescope; a controls model that models both controller dynamics and noise; an optics model to accurately demonstrate performance and optical feedback; and loads models to characterize various environmental loads.

This paper will introduce the GMT integrated modeling architecture, but will focus on the specific tools and process developed to build the critical structural model. An efficient process was required to support the variety of required analyses, update frequency of underlying finite element models, and various project critical trade studies. The end-to-end process, from subsystem finite element models to a system level plant and Simulink block diagram has been achieved through development of a new MATLAB class with many useful functions. Functions are covered that combine the subsystem models, manipulate those models, and help them run efficiently in discrete and continuous time. Verification and version control are also discussed. Case study of wind is presented with preliminary performance results.

TABLE OF CONTENTS

1. INTRODUCTION

The Giant Magellan Telescope (GMT) is a broad bandwidth optical telescope that achieves a 24m diameter aperture with seven 8.4m diameter primary mirrors. It is part of the latest generation of optical telescopes, which are all considered Extremely Large Telescopes (ELTs). Based on the current schedule it will have first light in 2023, which is the first of the 3 ELTs.

An image of the system level finite element (FE) model of the GMT and the concrete pier (light blue) is given in Figure 1. The enclosure that houses the telescope, protecting it from the environment, is not shown.

Though the GMT has many unique characteristics, two features distinguish it from the other ELTs. First, there are seven large circular primary mirror segments, as opposed to 798 smaller hexagonal segments on the European Extremely Large Telescope (E-ELT) and 492 hexagonal segments on the Thirty Meter Telescope (TMT). This optical configuration means that GMT has fewer sharp edges

978-1-5386-2014-4/18/$31.00 ©2018 IEEE

resulting in a cleaner point spread function (PSF) than the other proposed ELTs.

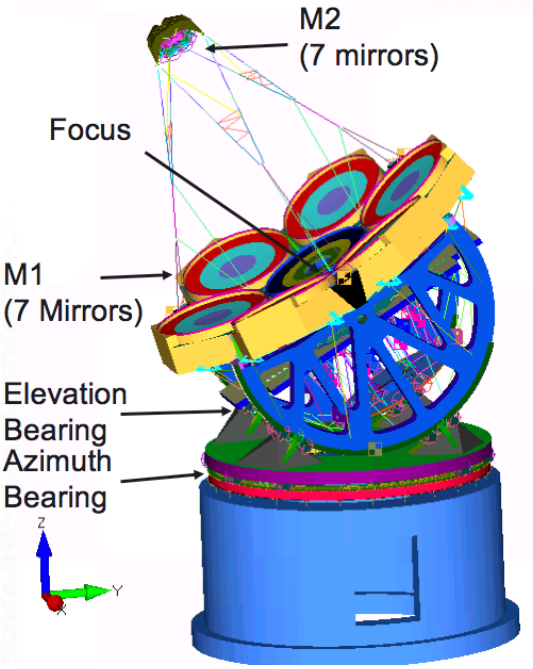

Figure 1. The system level finite element model of the Giant Magellan Telescope.

Second, both the primary and secondary mirrors are segmented, which makes it especially challenging to phase both sets of mirrors using wavefront sensors.

Integrated modeling is a process that has been adopted in recent years in the telescope industry to bring different aspects of modeling telescopes, such as CFD, thermal, structures, controls and optics closer together, so that iterations in a design, or changes in requirements can be evaluated with minimal cost. The process is most commonly used for [1]

- Global design specification
- Error budgets
- Sub-system requirement definition
- Inter-system design trade-offs

Each project implements integrated modeling in a different way. Integrated modeling was considered a critical element of James Webb Space Telescope (JWST) [2]. It was used primarily to support engineering design and verification of high level optical requirements for image quality. Separate integrated models were produced for wind jitter and so-called structural-thermal-optical (STOP) modeling.

In the Thirty Meter Telescope (TMT) and the Large Synoptic Survey Telescope (LSST), the integrated model used is not as seamlessly integrated as for JWST [3-4]. The models were used to produce budgets and, in the case of wind jitter, demonstrate design compliance with requirements.

The GMT Organization (GMTO) has fully embraced the integrated modeling paradigm. The Systems Engineering group, along with the chief engineer, is developing and flowing down science and operational requirements and is the guardian of the performance budget. An integrated performance model of the telescope is being developed to support requirements derivation, performance assessment and trade studies that drive telescope architecture decisions. This model has four key elements; a structural plant model which exhibits the complex dynamics of the telescope; a controls model with including controller, actuator/sensor dynamics, and actuator/sensor noise; an optics model to accurately demonstrate performance and optical feedback; and environmental loads that are generated outside the integrated model. Figure 2 illustrates an example of how these different elements work together in integrated models at GMTO.

We are developing/have developed tools to automate or increase efficiency of our modeling procedures. The goal of this paper is to introduce the tools that have been developed to create structural plant models from the FE model that meet the needs of the integrated modeling team to efficiently create, update and maintain integrated models. A description of some of the direct uses of these tools is shown in Figure 3. The process a) includes the functions used to convert a Finite Element (FE) model into a mathematical structural plant

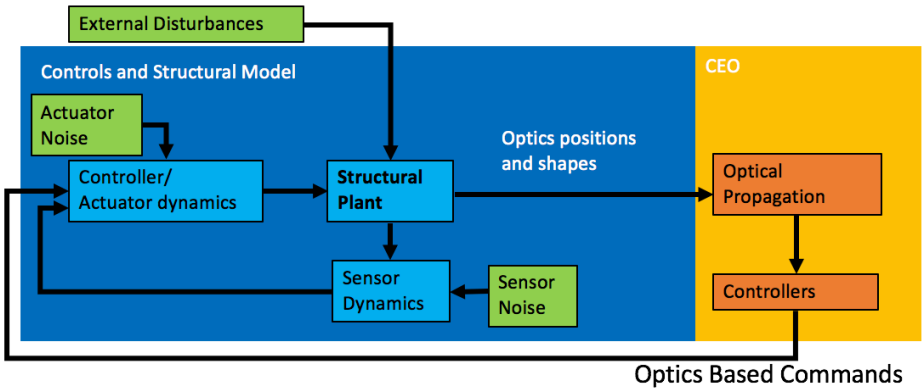

Figure 2. Integrated Model architectures at GMT

model. Process b) includes tools developed to work with a high order structural plant to make Bode plots, which is useful to controls engineers. Process c) shows the use of the function that can easily recover the static gain from the plant model.

Section 2 of this paper introduces the fully formed integrated model itself.

Sections 3-7 cover the structural modeling tools that are the topic of this paper. Section 3 reviews the modal reduction process NASTRAN uses to reduce individual subsystem models into a mathematical model that can be imported into MATLAB. Section 4 covers the MATLAB class structure which stores the mathematical plant model, as well as the methods that operate on this model. Section 5 covers how the CMM class is created from the output of the FE model run. Section 6 covers the most important methods of the CMM class. Finally, Section 7 covers the process by which these are all put together to build the structural plant.

Section 8 covers the topics of process control, including model requirements, configuration management, verification and validation.

Sections 9 reviews a case study of how these tools are currently being used in the wind analyses. Preliminary results are also presented.

Overall these tools are proving to be useful and necessary for performing a variety of the analyses required for proceeding through the remaining phases leading up to the commissioning of the telescope.

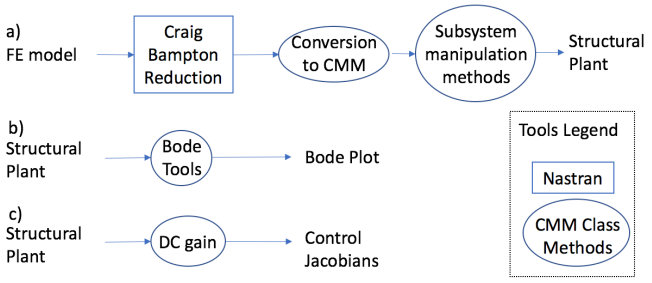

Figure 3. The tools used in building, manipulating and utilizing the structural plant model.

2. GMT Integrated Model Overview

The integrated model is broken into 4 parts: structural, controls, loads and optics. It is implemented either in discrete time, or in the frequency domain (for linear models).

The structural plant is the mathematical representation of the main structural components of the model as derived from FE models. It is one of the focuses of this paper.

The controls model includes dynamic equations representing the controllers as well models for actuator and sensor dynamics. The models can include non-linear features as well. Controllers are made to be robust at this stage of the design, by allowing for ample phase margin, and using conservative damping assumptions for the structural plant.

The loads vary based on the specific analysis target. Generally, they require various other software packages, and complementary inputs in the structural plant. The load types can be broken up by frequency regime. Quasi static loads are caused by installation tolerances and temperature variance. The loads between 0 and 20 Hz are largely caused by wind and seismic fluctuations. Loads above 20 Hz are mostly caused by pump vibration and motor cog.

The optics model is used to model the active and adaptive optics telescope systems, as well as introduce the effects of atmospheric disturbances. The primary optics tool used at GMT is built using an open-source tool that is being developed in-house– the CUDA-Engined Optics (CEO) simulator. This tool can be called directly from Simulink. It uses cloud GPU's to make ray tracing calculations many times faster than existing off the shelf software. For linear analyses, such as the implementation of the line-sight-equations, computations can be done efficiently without the use of CEO. The wind case study in Section 10 uses the linear approximation.

3. Craig-Bampton Reduction

In FE models, dynamic systems are represented using the second order form:

$$M\ddot{x} + D\dot{x} + Kx = Pu \tag{1}$$
$$y = Lx$$

where $M, D,$ and K, are the mass, damping and stiffness matrices respectively, u represents the input loads, and y represents the output degrees of freedom.

In this paper, the number of degrees of freedom (DOF) in the FE models is reduced using a Craig-Bampton transformation. This is a common approach in the aerospace industry, and results in reduced order models that retain exact interface stiffness combined with dynamic response over some frequency range. The Craig-Bampton method starts with the FE equations of motion for the component partitioned into interface and interior DOF, and reduces it to the interface (A) DOF plus modal (O) DOF:

$$\begin{bmatrix} M_{AA} & M_{AO} \\ M_{OA} & M_{OO} \end{bmatrix} \begin{Bmatrix} \ddot{x}_A \\ \ddot{x}_O \end{Bmatrix} + \begin{bmatrix} D_{AA} & D_{AO} \\ D_{OA} & D_{OO} \end{bmatrix} \begin{Bmatrix} \dot{x}_A \\ \dot{x}_O \end{Bmatrix} + \begin{bmatrix} K_{AA} & K_{AO} \\ K_{OA} & K_{OO} \end{bmatrix} \begin{Bmatrix} x_A \\ x_O \end{Bmatrix} = \begin{bmatrix} P_A \\ P_O \end{bmatrix} u$$

$$y = \begin{bmatrix} L_A & L_O \end{bmatrix} \begin{Bmatrix} x_A \\ x_O \end{Bmatrix} \tag{2}$$

where the inputs u are defined by the static loads defined in the FE model and the outputs y are the requested

displacement output degrees of freedom. The Craig-Bampton transformation is:

$$\begin{Bmatrix} x_A \\ x_O \end{Bmatrix} = \begin{bmatrix} I & 0 \\ [G_{OA}] & [\Phi_O] \end{bmatrix} \begin{Bmatrix} x_A \\ x_Q \end{Bmatrix} \quad (3)$$

Where:

$[G_{OA}]$ - Constraint shapes calculated as $-[K_{OO}]^{-1}[K_{OA}]$

$[\Phi_O]$ - Mode shapes with interface DOF fixed, including residual vectors for applied loads

x_Q - states associated with modes where interface DOF is fixed and associated with residual vectors for internal loads

The reduced order model has the following form:

$$\begin{bmatrix} \bar{M}_{AA} & M_{AQ} \\ M_{QA} & I \end{bmatrix} \begin{Bmatrix} \ddot{x}_A \\ \ddot{x}_Q \end{Bmatrix} + \begin{bmatrix} \bar{D}_{AA} & D_{AQ} \\ D_{QA} & D_{QQ} \end{bmatrix} \begin{Bmatrix} \dot{x}_A \\ \dot{x}_Q \end{Bmatrix} + \begin{bmatrix} \bar{K}_{AA} & 0 \\ 0 & \Omega^2 \end{bmatrix} \begin{Bmatrix} x_A \\ x_Q \end{Bmatrix} = \begin{bmatrix} P_A \\ [\Phi_O]^T P_O \end{bmatrix} \{u\}$$

$$\{y\} = [L_A + L_O[G_{OA}] \quad L_O[\Phi_O]] \begin{Bmatrix} x_A \\ x_Q \end{Bmatrix} \quad (4)$$

The Craig-Bampton reduction has been found to be a very robust way of reducing components for assembly into system models [6]. The interface DOF exactly capture the interface stiffness, while the modal DOF capture internal dynamics. Including residual vectors also accounts for the contribution of all the truncated modes to the internal static response. This results in a compact reduced model that accurately captures all the behavior of the component through a specified frequency range.

In the reduction process, one must be clear about the following features:

- Subsystems included
- Frequency range
- Boundary nodes
- Inputs, including but not limited to
  - Forces
  - Moments
  - Pressure patches
  - Thermal maps
- Outputs, typically
  - Nodal degrees of freedom
  - Linear combinations of nodal degrees of freedom (such as line of sight equations)

Each of these characteristics often change to meet the needs of an integrated model. For example, the Craig-Bampton reduction is generally considered accurate up to half of the maximum frequency considered. If the system does not pass control robustness requirements due to model uncertainty, then extra frequencies should be included.

One interesting feature of a Craig-Bampton model is that, unlike in a simple modal reduction, the resulting mass and stiffness matrices are not diagonal. Figure 4 demonstrates the form of the sparse matrices produced in a Craig-Bampton reduction. This is the output of MATLAB's *spy* command, where nz is the number of nonzero elements of the matrices. In this example, the first 50 degrees of freedom are boundary degrees of freedom. This has the effect that the first 50 rows and columns of M are not sparse, and only the top 50x50 partition of K is not sparse. The remaining modes and residual vector degrees of freedom account for the diagonal lower right partition of both M and K matrices.

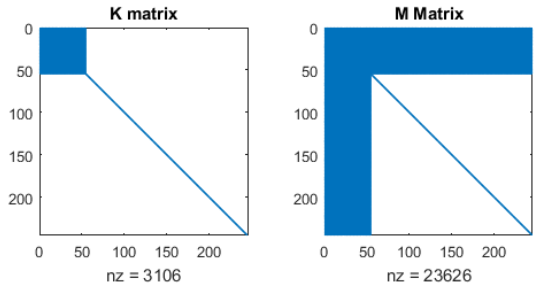

Figure 4. Matrix form of Craig-Bampton *K* and *M* matrices. The X and Y axes represent column and row matrix index respectively.

4. Component Mode Model Class

The Component Mode Model (CMM) class was built by GMTO and ATA to facilitate working with the high-order subsystem models being generated for a variety of analyses. The class properties encapsulate the elements that are important to the model such as inputs, outputs, system variables, and meta data which stores the history of the model. The class includes many methods to manipulate the models. It allows for the combination of subsystems together and retains meta data through the operations.

Overall there are currently 16 functions and only the most important are covered in Section 6.

A struct stores the matrices $A, B, C,$ and D from the model's state-space form:

$$\dot{x} = Ax + Bu$$
$$y = Cx + Du \quad (5)$$

which represents the same dynamics as the form in equation (1). Note, for this equation and those that follow, D holds a different meaning from equations (1-4). In this case, the x vector is still the state vector in the equation but it contains twice as many states as in equation (1), since it is a first-order form representing the same dynamics.

The model can alternatively be stored as a discrete time model:

$$x(k+1) = Ax(k) + Bu(k)$$

$$y(k) = Cx(k) + Du(k)$$

$$x(k) = x(t_k), t_k = T_s k \tag{6}$$

where k is an index, T_s is the sampling time.

5. Conversion To CMM

To create a CMM object from a Craig-Bampton reduced model, the model must first be converted into a state-space representation of the form given in (5). The function *op42SS* was written to perform this conversion. This function takes the binary NASTRAN output file (.op4) that is generated by the NASTRAN model reduction, the NASTRAN master file used to make that reduction, as well as an optional matrix denoting which node velocities should be included in the state-space representation, and outputs a state space system.

The function first reads the NASTRAN input and output files using the ATA IMAT function *readnas* [7]. This gives the K, M, P, and L matrices from (1), as well as the boundary and fixed base modal degrees of freedom. These matrices are converted into state-space form:

$$\begin{bmatrix}\dot{x}\\ \ddot{x}\end{bmatrix} = \begin{bmatrix}0 & I\\ -M^{-1}K & 0\end{bmatrix}\begin{bmatrix}x\\ \dot{x}\end{bmatrix} + M^{-1}[P \quad P_{BSET}]u$$
$$y = \begin{bmatrix}L & 0\\ 0 & L_v\end{bmatrix}\begin{bmatrix}x\\ \dot{x}\end{bmatrix} + 0 \tag{7}$$

P_{BSET} has been added to (1) and is a matrix of ones and zeros that allows forces to be applied to the boundary degrees of freedom. L_v is added here in case any velocity degrees of freedom are requested.

Once a state-space representation of the Craig-Bampton reduced model is created, the resulting matrices are used to create a CMM object.

6. CMM Methods

This section includes a survey of the most important methods in the CMM class. Other notable methods include; a function that trims the available input and output indexes, a function that animates a 3D model in MATLAB, a transfer function plotting utility that uses the second order form to save computation cycles, and a model truncation method.

createSimulink()

The *createSimulink()* function generates a Simulink subsystem block with inputs and outputs properly labeled, as shown in Figure 5. This is speeds up the process of identifying indexes for transfer function plots and for connecting subsystems. The input/output channels are displayed in brackets, while the number of inputs for each are in parentheses. This option is also available with an implementation using the second order form, which speeds up the time-domain computations significantly.

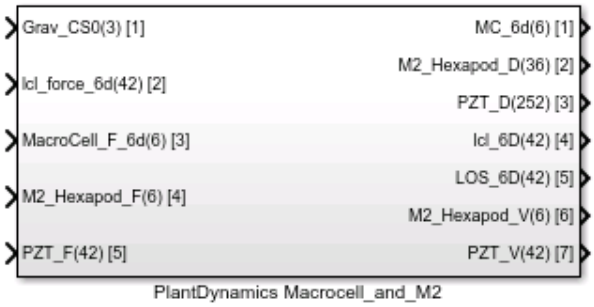

Figure 5. Subsystem Simulink CMM block.

Connect(), ground(), internal_spring()

These three functions all implement the same mathematical concept (as demonstrated in in Figure 6) of connecting output displacements to inputs forces through springs, but are used for different specific scenarios. The equations presented in this section work for both continuous and discrete time models, although the types cannot be mixed.

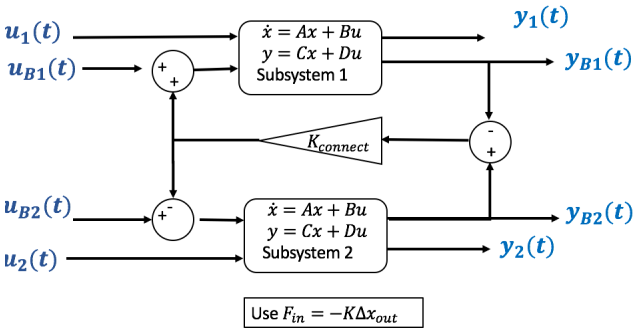

Figure 6. Graphical representation of connecting two models with springs.

The *connect()* function connects two subsystems together using springs. To connect two systems with a spring, consider two state-space systems described by the matrices $\{A_1, B_1, C_1, D_1\}$ and $\{A_2, B_2, C_2, D_2\}$ respectively. In this state, the full dynamics of both systems are represented, but no connection has been made. The combined system can be described by the matrices:

$$A = \begin{bmatrix}A_1 & 0\\ 0 & A_2\end{bmatrix}, B = \begin{bmatrix}B_1 & 0\\ 0 & B_2\end{bmatrix}$$
$$C = \begin{bmatrix}C_1 & 0\\ 0 & C_2\end{bmatrix}, D = \begin{bmatrix}D_1 & 0\\ 0 & D_2\end{bmatrix} \tag{8}$$

Let the input and output indices for the connected degrees of freedom be i_1 and o_1 for system 1 and i_2 and o_2 for system 2. And let the number of states in system 1 be N_1. Then the force applied on system 1 by system 2 and the force applied on system 2 by system 1 are:

$$F_{12} = -k(C(i_2) - C(i_1))x$$
$$F_{21} = -k\big(C(i_1) - C(i_2)\big)x \tag{9}$$

so that:

$$B_c(o) = B(o) - kB(o)\big(C(i_1) - C(i_2)\big) \text{ for } o \text{ in } o_1$$
$$B_c(o) = B(o) - kB(o)\big(C(i_2) - C(i_1)\big) \text{ for } o \text{ in } o_2$$
$$B_c(o) = B(o) \text{ otherwise} \quad (10)$$

where $B\_c(\mathrm{o})$ and $B(o)$ are row o of the B matrix for the connected and unconnected systems, and k is the stiffness of the springs. The same set of equations are used for *internal_spring()* (without the need to first combine systems).

In the case of the function *ground(),* one side of the spring is grounded which is modeled by changing the equation by setting $\mathrm{C(i_2)}$ is 0, and the set o_2 is empty.

It is possible to connect two degrees of freedom without a spring, which effectively removes a degree of freedom, but that function is not included. Instead, for a direct connection, stiff springs are used.

convert_to_modal()

In general, the A matrix resulting from the conversion from mass and stiffness matrices, and combination of subsystems, has no specific form. It is convenient to have A in a sparser form for the sake of adding damping, converting to the more efficient second order form, and for modal truncation. We call this form the modal form.

The transform to the modal form is done as follows:

$$x_m = T_m x,\ A_m = T_m^{-1} A T_m,\ B_m = T_m^{-1} B,\ C_m = CT \quad (11)$$

where A is broken up into n second order equations:

$$A_m = \begin{bmatrix} A_1 & 0 & 0 \\ 0 & \ddots & 0 \\ 0 & 0 & A_n \end{bmatrix}$$

$$\text{where } A_i = \begin{bmatrix} 0 & 1 \\ -\omega_i^2 & -2\zeta_i\omega_i \end{bmatrix} \quad (12)$$

and ω_i and ζ_i and the resonant frequency and damping of the ith mode.

While the A_m matrix is easy to compute, the transformation matrix T_m is non-trivial. A simple eigenvalue decomposition does not directly work because Simulink requires real-valued matrices for simulation.

The transformation matrix from an arbitrary set of states requires 2 individual transformations and some sorting.

First, ω and ζ are found using the odd eigenvalues of A, λ_{odd} (using the MATLAB function eig):

$$\omega = |\lambda_{odd}|$$
$$\zeta = 1 - \left| \frac{\tan^{-1}\left(\frac{Imag(\lambda_{odd})}{-Real(\lambda_{odd})}\right)}{\frac{\pi}{2}} \right| \quad (13)$$

Then A_m is populated using these frequencies and damping values.

Next, let $\mathrm{A_a, T_a}$ be the diagonalized form of A and the transform such that $\mathrm{x_a = T_a x}$. The rows of $\mathrm{A_a}$ and $\mathrm{T_a}$ are re-ordered in the same way, so that the diagonal values of $\mathrm{A_a}$ are sorted.

Let $\mathrm{A_b, T_b}$ be the diagonalized form of $\mathrm{A_m}$ and the transform such that $\mathrm{x_b = T_b x_m}$. Then, $\mathrm{A_b}$ is sorted by absolute value along the diagonal, along with re-sorting $\mathrm{T_b}$. Thus, if modes are spaced enough that modes are not re-ordered due to numerical uncertainty, then $\mathrm{x_a = x_b}$.

Then the transformation to modal coordinates is:

$$T_m = T_b^{-1} T_a \quad (14)$$

Then B_M and C_M (B and C matrices associated with A_M) are calculated:

$$B_m = T_a^{-1} T_b, C_m = T_b^{-1} T_a \quad (15)$$

This method can be incorrect if two modes numerically have the same frequency but different damping. A check is needed to verify that mode shapes associated with x_1 and x_2 are also equivalent.

add_damping()

Once the A matrix is in modal form, then damping can be easily applied as a function of frequency by adjusting the ζ values.

bode_second_order_d(), create_simulink_secondorder()

Once in modal form, the model can be broken into n second order state-space systems:

$$\dot{x_i} = A_i x_i + B_i u$$
$$y = Cx \quad (16)$$

where B_i is the ith row of B.

For now, the Tustin transformation is used both for frequency and time domain second order implementations. Thus, to find the transfer functions the substitution is made using the Tustin transform:

$$s = \frac{2}{T_s}\frac{z-1}{z+1} \quad (17)$$

For displacement inputs, each transform is:

$$h_i(z) = \frac{(z+1)^2}{(z-1)^2}\frac{T_s^2}{4} + 2\frac{2}{T_s}\zeta_i\omega_i(z^2-1) + \omega_i^2(z+1)^2 \quad (18)$$

and for velocity states this is multiplied by a derivative

$$h_{iv}(z) = \frac{2}{T_s}\frac{z-1}{z+1}h_i(z) \quad (19)$$

The discretization can also be performed with a zero-order hold. The conversion to second order form is done to improve computation time.

bode_second_order_d() computes the discrete time transfer function, given requested inputs, outputs and frequencies. *create_simulink_secondorder()* works like *createSimulink()* but instead of using a state-space block, implements *n* second order difference equations.

dcgain()

This function determines the static gain of each channel of the system. This is extremely useful for diagonalizing MIMO control loops by using the output to find Jacobian matrices. The math is straightforward:

$$DCgain = -CA^{-1}B + D \tag{20}$$

for continuous time systems and

$$DCgain = -C(A - I)^{-1}B + D \tag{21}$$

for discrete time systems, where I is an identity matrix.

7. Model Reduction Process

The following describes in detail the process by which the system level FE model is converted into the structural plant model.

Step 1: FE Model Preparation

The system level structural FE model (in Figure 1) is the starting point in this process. First, the initial decisions must be made about which subsystems are included, and which boundary nodes, inputs, outputs and frequency ranges are used. Necessary input and output coordinate system are added and/or double checked. The suitability for any the analysis is considered, and detailed subsystems are used where necessary. Sometimes, nodal renumbering is necessary to have inputs and outputs grouped conveniently.

Step 2: Run NASTRAN

At this point the NASTRAN model is run using solution 103, with residual vectors requested, and with superelement output to an output 4 file.

Step 3: Build Subsystem CMMs

This is described in detail in Section 5 and an example of the resulting Simulink block from a subsystem is shown in Figure 5.

Step 4: Ground and combine models

Using previously discussed functions, the subsystems models are combined with springs, and other parts of the model are grounded as necessary.

Step 5: Add Damping

The model is converted into modal form and damping is applied on a frequency by frequency basis. Damping can also be included in the output of FE model. For the needs of GMTO, however, it is convenient to have damping as an easily adjustable feature implemented at this step.

Step 6: Trim Outputs

The default input and output degrees of freedom to NASTRAN superelement are typically numerous and it is helpful to remove extraneous ones.

Step 7: Discrete Second Order Form

The sampling time is picked so that the Nyquist frequency is adequately above the frequency cut off. This way there is also not much effect from aliasing. Aliasing can be addressed either by adding anti-aliasing low pass filters, or through modal truncation.

8. Process Control

As the model is being developed it is helpful to have controls in place to maintain consistency across analyses and throughout the life of the project.

FE Model Requirements

A requirements document is written so that the system level FE model maintains certain features as subsystems are updated to match design changes. Requirements include:

- NASTRAN input file breakdown by telescope subsystem
- Node and Element identification number (ID) ranges
- Coordinate system definition
- Specific Node ID for optical outputs

Configuration Control

The integrated model is stored in several GIT repositories, with released versions for any significant changes or bug updates. The system level FE model, and the detailed M1 model are also under version control. Other subsystems do not have detailed FE models. GIT works well for NASTRAN input files since they are ASCII. In some cases, large binary files must be saved elsewhere, typically a Docushare directory mirroring the GIT directories.

Verification

Verification has not fully been codified into the process. In the requirements document, specific requirements are included to verify that the model itself is up to typical finite element modeling standards. Requirements include:

- Model checks passed for released versions
- Point verification tests

Other forms of verification that have been employed are:

- Peer Review
- Formal IM reviews

An example of verification is shown in Table 1. In that table, the modal frequencies from the FE model with the base of the pier fixed, and with stiff springs connecting the drive rotors, is compared to those after the model is processed through the steps in the previous section. The table demonstrates that the tools provide adequate results. Other verification cases include the calculation of the Jacobian using the static gain matrix. These types of verification tests have proved useful for most analyses to date, though a mesh refinement verification may be required for analyses at higher frequencies.

Table 1. Modal frequency comparison as example of model verification.

Mode #	FEM (Hz)	continuous time state-space (Hz)	discrete time state-space (Hz)
1	0	0.13	0.08
2	0	0.15	0.09
3	0	0.21	0.13
4	3.24	3.24	3.24
5	4.51	4.51	4.51
6	6.77	6.77	6.77
7	7.6	7.6	7.6
8	7.96	7.97	7.97
9	8.47	8.47	8.47
10	8.61	8.62	8.62

Validation

Validation studies for the structural model are being considered by applying the same methodology to modeling existing partner telescopes, and comparing model results to data collected on those telescopes.

9. Case Study: Wind Jitter

Wind jitter is a critical requirement. It is defined as the tracking performance with only the wind load applied. Thus, the structural response is coupled with the effects of all closed loop controls.

The image quality is split into two terms – blur and figure. The blur term accounts for the difference in the line of sight pointing for the seven segments from desired. The figure term adds in the effects of imperfect shape of individual segments. Only the image blur is considered here.

In this case study, the wind generation of wind loads are considered first. Then the FE model used for this specific requirement is described. The next 5 subsections are devoted to the subsystems considered in the analysis: main axes, M1 and M2. And the last subsection describes the preliminary results for natural seeing. Natural seeing is the control mode that does not use adaptive optics.

Wind Loads

The greatest challenge for the TMT integrated model was the development of an accepted set of wind loads [8]. Methods were developed to convert steady state CFD results to force spectra on the structure. The same methods are being used to develop loads at GMTO. The CFD derived loads are converted into non-correlated forces and moments at various points in the structure including:

- M2
- 6 areas along the truss
- Each M1 mirror
- Each M1 cell

This methodology is thought to give a good approximation of the loads that the system will have. An example a spectrum applied to M2 is shown in Figure 7. The desired spectrum is shown in red, and the spectrum of the applied time-domain signal is shown in blue. Most of the energy is below 10 Hz for all loads.

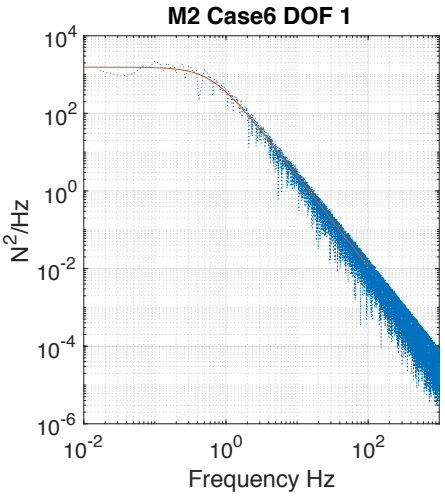

Figure 7. Example Input Load Spectrum.

FE Model General Description

The system level FE model is shown in Figure 1. That model is broken into two subsystems for the purposes of this case study. The M2 model, shown in Figure 8, is defined as one subsystem, with fixed base modes defined up to 300 Hz. The remainder of the model is used as the second subsystem, with fixed base modes defined up to 50 Hz. These ranges were determined after an iteration through the process suggested that the resulting model uncertainty caused the controllers not

to be suitably robust. The model itself has 2093 modes. The first few modes are shown in Table 1. The distribution of the modes in this reduced model is shown in Figure 9. Each bar of the histogram represents a 10 Hz range. It is evident that the modal density ramps up after 10 Hz. In reductions in which the mount frequency range is higher the modal density continues to climb.

We are using a value of 1 percent of critical damping, but controllers are tuned to have adequate margins down to 0.25% of critical.

The mass of major components of the structural FE model are shown in Table 2. The structures that the control systems must hold in place with precession are indeed massive.

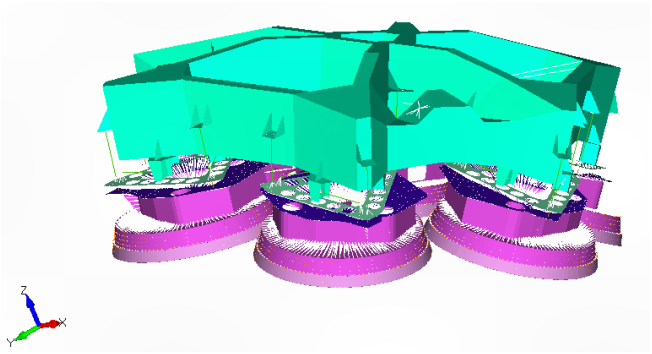

Figure 8. FE model of the M2 subsystem. The "Macrocell" is shown in aqua. Each M2 segment cell in purple.

Table 2. GMT Mass distribution (all units in metric tons)

	Top Level	Level 2	Level 3
Pier	**4280**		
Optical Support Structure (OSS)	**938**		
Truss		19	
M1		340	
M1 (Each weldment)			32
M1 (each Mirror)			**17**
M2		6	
GIR		118	
GIR structure			56
Instruments			61
Telescope mass	**1378**		
Total Mass	**5658**		

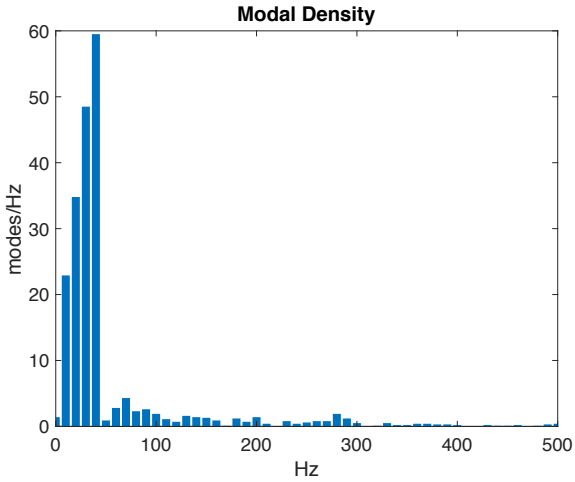

Figure 9. Modal Density Plot.

Mount Axes

The mount controls the 3 main degrees of freedom of the telescope. The azimuth drives control rotation about zenith along the azimuth bearing. The elevation drives control rotation of the optical support structure (OSS) about the elevation axis parallel with the ground. Finally, the Gregorian Instrument Rotator (GIR) is located inside the OSS. It rotates about the direction of sight of the telescope, so that the orientation of the sky remains constant in the focal plane. The azimuth and elevation axes have 4 drives and 4 encoders each. The GIR axis has 2 drives and 2 encoders.

In the system level FE model, each of these axes are represented using stiff springs at the drives. This effectively represents a system with infinite control bandwidth for dynamic solutions. Thus, for model reduction in the integrated model, the springs representing these axes are removed. The structural plant model represents inputs to each of the 10 drives as forces, and outputs as local displacement. Each mount axis has a cylindrical coordinate system associated with it, so that the input forces and output tangential motions are trivially included as inputs and outputs of the reduced order model.

The controls model is then built to add in appropriate sensor and actuator dynamics and controllers with appropriate bandwidth. For now, the drives only control the main axes, but they are expected to also actively dampen the first 2 telescope modes.

The motors of the azimuth axis and the elevation axis can be modeled as a single pole low pass filter with the pole placed at 55Hz, in series with a delay:

$$M(s) = \frac{2\pi 55 e^{-\Delta t s}}{s+2\pi 55} \tag{22}$$

The encoder is simulated as a unity gain with a transport delay of Δt, where $\Delta t = 0.002$ seconds.

$$Enc(s) = e^{-\Delta t s} \tag{23}$$

The first two modes of the telescope (with drive rotors fixed) are shown in Figure 10 and Figure 11. The first flexible modes of the structure tend to limit the performance of the control system, so it is helpful to understand them. The transfer function from azimuth applied force at the drives to local tangential motion is shown in Figure 12. At about 2 Hz, the second order pole is evident that is caused by adding "soft" springs to the Azimuth axis, and is not realistic. Between .2 and about 3 Hz, the system acts like a double integrator. The first resonant peak is at about 8 Hz, and is a truss bending mode. An integral controller is placed to achieve a bandwidth of about 1.5 Hz, bandpass filters are in place to stabilize the low order modes, and notch filters reduce the effect of the higher order modes. The resulting sensitivity function (the inverse of 1 plus the loop gain) is shown in Figure 13. This figure is used to demonstrate the controllers' ability to reject disturbances. Note what appear like notches at 7 and 9 Hz show the effect of close to 0 phase at the peaks of the modes in the loop gain. This results in the azimuth drives successfully damping these modes. The elevation and GIR axes have controllers with a bandwidth of about 1 Hz each.

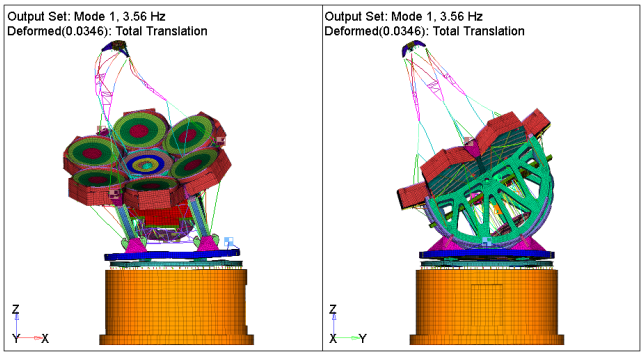

Figure 10. Mode 1 – Lateral Bending – 3.56 Hz

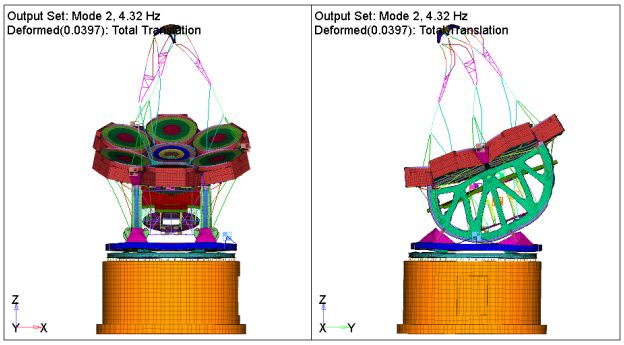

Figure 11. Mode 2 – Fore-Aft Bending – 4.32 Hz

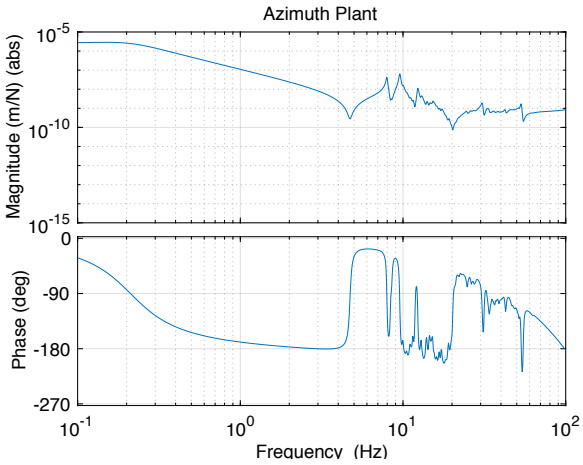

Figure 12. Azimuth Plant Transfer Function.

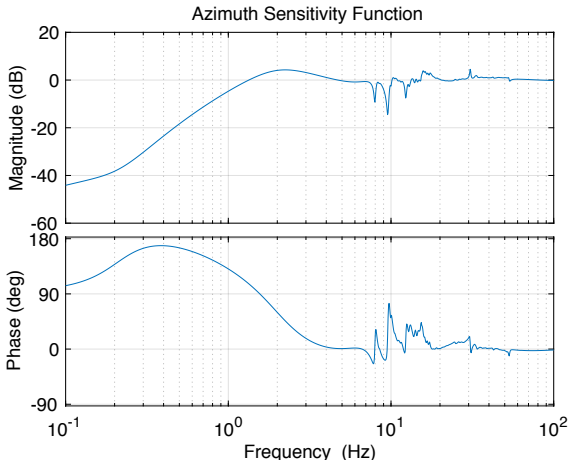

Figure 13. Azimuth Sensitivity Function.

M1 Subsystem

The M1 mirrors are 8.4m diameter borosilicate glass. They have two thin face plates and internally have a honeycomb structure.

The M1 subsystem is based on the design concepts inherited from the support systems for the borosilicate glass mirrors on Large Binocular Telescope (LBT) and the Large Synoptic Survey Telescope (LSST). When in tracking mode, the mirror is supported in two ways as shown in Figure 14. The six Hardpoints in a segment cell weldment are stiff actuators that form a hexapod. They control the rigid body position of the each M1 segment. There is a bed of over 300 pneumatic actuators for each M1 segment that offload the Hardpoints, so that gravity loads and low frequency wind loads are transmitted evenly into the cell weldment. They do this by closing a loop that minimizes the signal from strain gauges on the Hardpoints. Additionally, these actuators are used to correct any measured figure error through the active optics system. Outside the bandwidth of these loops, the Hardpoints provide the stiffness against wind loads.

The system level FE model uses a simple plate mesh model of the mirrors, with isotropic properties, as shown in Figure 16. The properties are tuned so that both the mass distribution and the first 2 modes match the detailed FE model when resting on the Hardpoints. The mirror is attached through rods representing the Hardpoints and does not include a representation of the actuators, thus it is difficult to use the FE model to simulate the design of the M1 subsystem. But, in the case of the wind jitter analysis discussed, we are not interested in figure error, so only require rigid body motions of the mirrors. The simplified mirrors from the system level FE model are used, and the actuators are modeled by equal and opposite forces and moments on the mirror shell and the top plate of the cell weldment as shown in Figure 15. This provides the effect of the evenly distributed forces from the actuators, while reducing model complexity. The Hardpoint strain gauge measurements are simulated by simply taking the difference between the two averaging elements.

The first flexible mode of the subsystem is at about 11 Hz, which is a combination of a side to side mode of the mirror with some flexing. The bandwidth of the Hardpoint strain gauge to actuator loop is about 1 Hz.

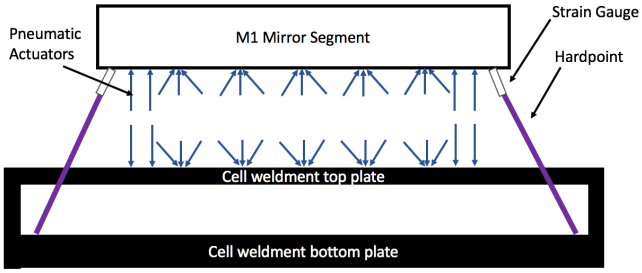

Figure 14. Cartoon of the design of the M1 cell (not to scale)

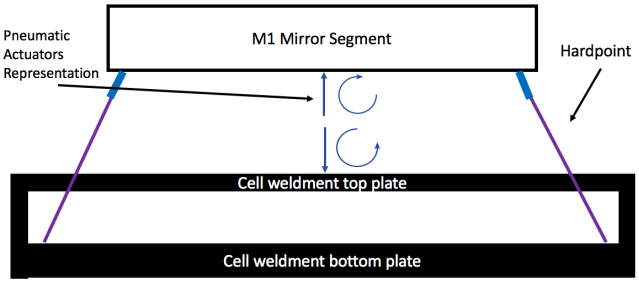

Figure 15. Cartoon of the method used in the latest version structural integrated model.

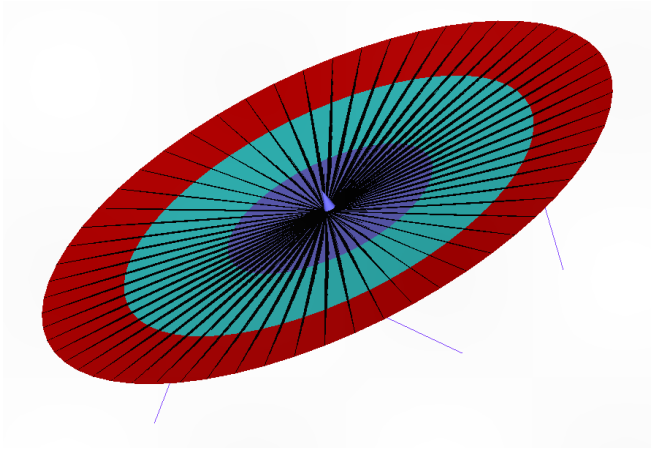

Figure 16. Simplified FE model of the a M1 mirror segment resting on its Hardpoints. The spider element in black is an averaging element that is used both to measure rigid body motion as well as distribute forces and moments applied to its dependent node.

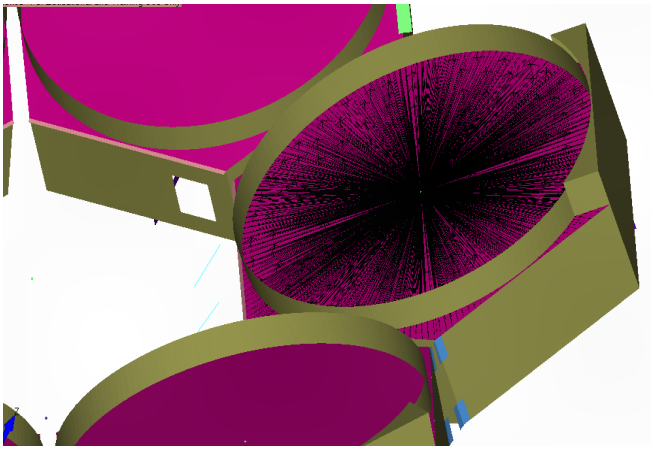

Figure 17. M1 cell weldment with top plate averaging element used for sensing and control.

M2 Subsystem

The M2 subsystem consists of two tiers. The Macrocell is supported by a large hexapod from above. The Macrocell in turn has 7 segment hexapods attached that hold the segment cells. These 8 hexapods change length as the elevation axis rotates the telescope to different zenith angles. In the Fast Steering Mirror (FSM) configuration, each segment cell holds a FSM via 3 piezo-electric (PZT) actuators that only control piston tip and tilt. This way they can be used to actively control the line-of-sight x and y focal plane motion of each M1/M2 segment pair (see next subsection for explanation of line-of-sight). Each cell also provides a dynamic vacuum that offloads the segment as the elevation axis rotates causing gravity deflection to change.

The system level FE model uses rods for both the hexapods and the PZT actuators. For the integrated model, the output coordinate systems of the nodes are defined in segment local

coordinates, so that it is easy to input forces and output displacements in the direction of action of the PZT actuators.

Line of Sight Equations

Each mirror has an output of its' rigid body motion. These are input to a linearized set of line-of-sight (LOS) equations to determine x and y focal plane motion.

Active Optics

The active optics is performed using the Acquisition and Guiding Wavefront Sensing System (AGWS). The AGWS consists of 4 identical probes, which each have two wavefront sensors that can be used for natural seeing. The first is used to correct focus, collimation, and M1 figure errors due to gravity flexure and thermal deformation, but only updates every 30 seconds. The other wavefront sensor senses tip-tilt for each of the seven segment pairs and is called the TT7 sensor. This sensor is the one modeled in the current wind jitter simulation, though the integrated model can be used to demonstrate the slow control loops as well.

The TT7 sensor is modeled using the linearized line-of-sight equations and applying a 6 ms delay that models the latency in the sensor.

The controller is an integrator, closed around each M2 segment set of PZT actuators. This is currently being done as a conservative approach, and with the latency, allows only a 7 Hz bandwidth for the closure of the loop.

Results

GMTO uses normalized point source sensitivity (PSSN) to form the image quality budget [9]. The post-processing method presented here is used to determine the RMS of the line-of-sight signals, instead of PSSN. The RMS method is a powerful tool for understanding characteristics of the results, and easy for engineers to execute, though final budgets are done in PSSN.

Simulations are run at 2000 Hz and 5 seconds' worth of data are collected. The power spectral density (PSD) results for global x line-of-sight are plotted in Figure 18 for several loop closure scenarios. For each scenario, this is calculated by first taking the seven individual line-of-sight signals, averaging them at every time point, and taking the PSD of the resulting signal. This plot is a rich source of information. For frequencies less than about 1 Hz, the effect of the mount axes and the tip-tilt control contribute up to a 6 order of magnitude decrease in the open loop power. The first dynamic resonance is at 3.5 Hz, which the mount axes effectively damp, but the M2 tip-tilt loop excites. Above 10 Hz, the plots converge because this is outside the controller bandwidths.

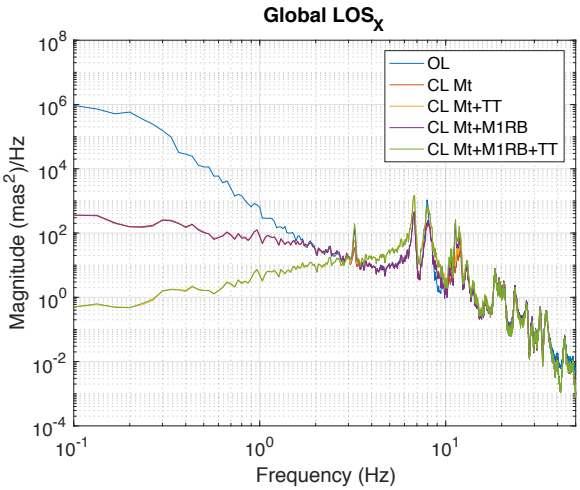

Figure 18. Global X line-of-sight PSD results.

Figure 19 shows the cumulative PSD results for the same test. The blue trace is the open loop result, and the other traces demonstrate the effects of closing other loops (Mt = mount axes, TT = M2 TT, M1RB = M1 force rebalance). This is computed by taking the cumulative integral, from low frequency to high frequency, and then taking the square root of the result at each frequency. A convenient result is that for a long enough time series and for a PSD with enough averaging, this total sum will equal the RMS of the time-domain signal. Thus, this plot is useful for identifying which frequencies contribute most to the RMS result. Though the tip-tilt loop causes a decrease in the cumulative PSD at low frequencies, above 8 Hz the dynamic amplification causes a greater decrease resulting in a greater RMS value for the signal.

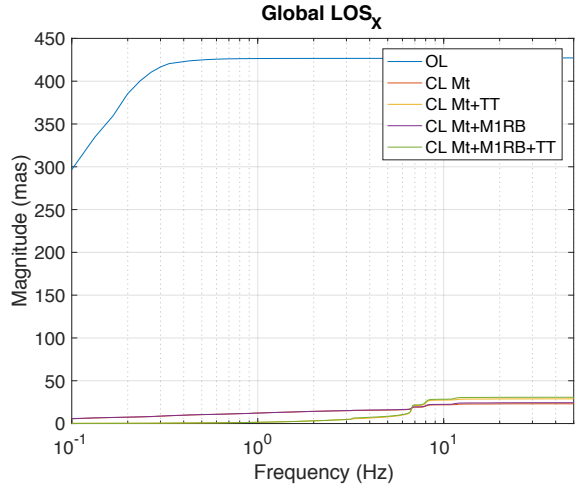

Figure 19. Global X LOS cumulative PSD results.

The full tip-tilt results are tabulated in Table 3. The first two columns show global tip-tilt. The remaining columns show segment tip-tilt. This is the result of taking the PSD of each raw line-of-sight time-domain signal and subtracting global

signal. This is the typical method that final results are presented, though sometimes only the last column is shown.

Table 3. Wind Jitter Natural Seeing Preliminary Results. (mas RMS)

DOF	Open Loop	Closed Loop		
		Mount	Mount +M1	Mount+ M1+ Active O
Glb X (mas)	427	23	24	31
Glb Y (mas)	1372	131	131	17
S1 X (mas)	12	12	14	17
S2 X (mas)	20	19	23	25
S3 X (mas)	18	18	21	23
S4 X (mas)	25	24	29	27
S5 X (mas)	13	13	18	22
S6 X (mas)	14	13	17	20
S7 X (mas)	15	15	17	22
S1 Y (mas)	9	9	12	15
S2 Y (mas)	15	14	17	21
S3 Y (mas)	18	16	19	25
S4 Y (mas)	10	10	14	17
S5 Y (mas)	14	12	14	19
S6 Y (mas)	13	12	16	20
S7 Y (mas)	7	7	8	11

10. Conclusions and Future Work

The tools developed provide a dynamic way to create versions of the integrated model for various uses. The wind case study has been used demonstrate the usefulness of the tools.

In coming months, many capabilities are scheduled to be added to the integrated model, as discussed in the following paragraphs.

A detailed model of an M1 mirror segment, with all individual hexagonal cells modeled as well as attachments for individual actuators, is currently in use at the subsystem level. Once it is made part of the integrated model, a representation of the shape of the surface of the mirror will be an output. This will allow the optics model to produce a PSF that also includes the effects of figure error. The model would also include the ability to control the M1 figure (at slow time scales), thus enabling the organization to better understand the active optics control loops involved and better set subsystem requirements.

There is currently a trade study being done to add active vibration damping to the support system for M2. Once this is better understood at the subsystem level, this will be modeled in the integrated models. The integrated model will then provide another iteration of the design of the so-called M2 Positioner.

The control system group is currently working on the codebase for the entire telescope. They plan to use a hardware-in-the-loop tests to verify the robustness of the code. The integrated model will provide the simulated plant for these tests.

Acknowledgements

The authors thank the all the GMT partners, without whom this project would not be possible. The authors would also like to thank Ben Irarrazaval, George Angeli, Antonin Bouchez, and Larry Sokolsky at GMT for providing support to the IM team. We'd like to thank Paul Blelloch and Matt Kaplan of ATA Engineering Inc. who were instrumental in providing support of the model reduction process in NASTAN.

References

[1] Andersen, Torben, and Anita Enmark. Integrated modeling of telescopes. Vol. 377. Springer Science & Business Media, 2011.

[2] Hyde, T. Tupper, et al. "Integrated modeling activities for the James Webb Space Telescope: optical jitter analysis." (2004).

[3] Angeli, George Z., et al. "Modeling tools to estimate the performance of the Thirty Meter Telescope: an integrated approach." Proceedings of SPIE. Vol. 5497. 2004.

[4] Angeli, George Z., et al. "Integrated modeling tools for large ground-based optical telescopes." Proceedings of SPIE. Vol. 5178. No. 9. 2003.

[5] Angeli, G. Z., et al. "An integrated modeling framework for the Large Synoptic Survey Telescope (LSST)." SPIE Astronomical Telescopes+ Instrumentation. International Society for Optics and Photonics, 2016.

[6] Craig, Roy, and Mervyn Bampton. "Coupling of substructures for dynamic analyses." AIAA journal 6.7 (1968): 1313-1319.

[7] IMAT, a suite of utilities for sharing data between MATLAB, analysis tools, and test software, Ver. 7.0, ATA Engineering, San Diego, CA, Oct 2017.

[8] MacMynowski, Douglas G., and Torben Andersen. "Wind buffeting of large telescopes." Applied optics 49.4 (2010): 625-636.

[9] Seo, Byoung-Joon, et al. "Analysis of normalized point source sensitivity as a performance metric for large telescopes." Applied optics 48.31 (2009): 5997-6007.

Biography

David Schwartz *received a doctorate from University of California, Los Angeles in 2010. Dr. Schwartz led ATA's effort to provide detail finite element analysis of the thermal distortion and stress of various configurations of the James Webb Space Telescope's star tracker assembly. He now is now the structural and controls engineer for the GMT integrated modeling group. For his postdoctoral research, he designed a novel micro-gyroscope that was used to win a successful DARPA contract for his lab.*

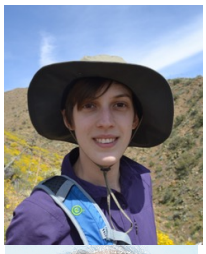

Kaylee Feigum *is a recent graduate from UC San Diego, with a Master's degree in Engineering Sciences, with a focus on controls and dynamics.*

Peter Thompson *is the Chief Scientist of Systems Technology Inc. located in Hawthorne, CA. He has a PhD in EE from the Massachusetts Institute of Technology. He has both theoretical and practical experience with control system design in a variety of disciplines including aerospace control, industrial control, and the control of large telescopes. He helped to develop both the original and the upgraded Az/El mount control system for the Keck 10-meter telescopes. He is part of the controls group for the Thirty-Meter-Telescope project and has worked on both the mount control system and the primary mirror control system. He has also developed the preliminary design of the mount control system for the CCAT 25-meter telescope for submillimeter wavelength astronomy.*

Clark Briggs *received a doctorate from Columbia University in 1978. He is the Director of the Robotics and Control group in ATA Engineering. Prior to joining ATA in 2009, he was a member of the engineering staff at the Jet Propulsion Laboratory, California Institute of Technology for 20+ years.*